THERMAL DEGRADATION OF BALLISTIC STEELS UNDER MULTIPLE IMPACTS: A THEORETICAL FRAMEWORK AND THE CUMULATIVE THERMAL DEGRADATION INDEX (CTDI) FOR ARMOX 500T

Pratih Mehta

Jadavpur University
Jadavpur, India
E-mail: pratih.mehta@jdvu.ac.in

Received: 25.02.2025. Approved: 10.04.2025.

Original Scientific Article

DOI: https://doi.org/65932/military-studies-2025-1-8
UDC: 355.4:623.41:623.463

Abstract: High-hardness armor (HHA) steels such as Armox 500T are qualified against single-shot threats, yet multi-hit studies show that repeated impacts within a limited footprint can degrade residual protective capacity in ways the single-shot paradigm does not capture. This paper develops a theoretical framework for the cumulative thermomechanical degradation of Armox 500T under repeated 7.62 × 51 mm NATO impacts and introduces the Cumulative Thermal Degradation Index (CTDI), a dimensionless predictor constructed from independently measurable or published inputs. The CTDI couples the Johnson–Cook constitutive response of Armox 500T (Iqbal et al., 2016; Saleh et al., 2018) with the Taylor–Quinney plastic-work-to-heat conversion framework revisited by Rittel et al. (2017) and with a one-dimensional thermal-relaxation model parameterized by published diffusivity data for martensitic steels. Hardness, fracture toughness and microstructural state appear only as validation outputs — never as inputs — removing the circularity that has complicated earlier cumulative-damage indices. The CTDI is validated against published datasets of Demir (2023) for Armox 600T and Saleh et al. (2018) for Armox 500T. Against Demir (2023) the CTDI shows Pearson $r = 0.993$ ($p < 0.001$, RMSE = 0.34 %); against Saleh et al. (2018) $r = 0.997$ ($p = 0.003$, RMSE = 0.11 %). Under hypothesis H1, localized heating can exceed the 720 °C recrystallization threshold for dense impact patterns with inter-shot intervals below approximately six seconds. The framework identifies inter-shot interval, overlap geometry and local plastic strain as dominant controls, and suggests that STANAG 4569 protocols may under-report residual-capacity loss for realistic short-burst engagements. All code, tables, figures and raw CTDI outputs are released as open supplementary material.

Keywords: *Armox 500T, high-hardness armor steel, multiple impacts, thermal degradation, Taylor–Quinney coefficient, Johnson–Cook model, cumulative damage; CTDI, 7.62 × 51 mm NATO, STANAG 4569, theoretical modeling.*

INTRODUCTION

High-hardness armor (HHA) steels occupy a central position in modern vehicle and personnel protection because they combine relatively low cost and good weldability with ballistic performance that rivals far more expensive monolithic ceramics over a broad threat spectrum (Hazell, 2015; Crouch, 2017). Among commercial HHA grades, SSAB's Armox 500T — a quenched and tempered martensitic steel nominally rated at 480–540 HBW — has become a reference material for light and medium

Military Studies: Journal for Strategy, Technology and Defence Sciences, Year 2025, Volume: 3, Issue: 1, Serial number: 3, p. 177 – 206.

armored vehicles, appearing both as a monolithic plate and as the metallic backing in hybrid systems (SSAB, 2023; Iqbal et al., 2016). Its constitutive behavior has been characterized extensively in the published literature, with Johnson–Cook parameters calibrated across quasi-static to SHPB strain rates and with thermomechanical response quantified up to several hundred degrees Celsius (Iqbal et al., 2016; Saleh et al., 2018; Iqbal et al., 2020).

Qualification of HHA plates against kinetic-energy threats is governed internationally by NATO STANAG 4569, which specifies projectile types, impact velocities, stand-off distances and, critically, a minimum spacing between shots intended to ensure that adjacent impact points do not interact mechanically or thermally (NATO, 2014). In practice, however, operational threat scenarios — particularly automatic small-arms bursts, crew-served weapons and short-range engagements — routinely produce impact patterns in which projectiles arrive within tens of centimeters and within fractions of a second of one another. Published multi-hit studies of Armox 500T and the related Armox 600T demonstrate that perforation limits, back-face bulging and residual hardness distributions measured under such dense patterns deviate systematically from single-shot predictions (Demir et al., 2023; Kılıç et al., 2014; Børvik et al., 2009). The deviation is consistently in the direction of reduced residual capacity, suggesting that a non-trivial fraction of the damage accumulated during a burst is not captured by simply summing the independent effects of each projectile.

The physical origin of this cumulative effect is well understood qualitatively. Every plastic deformation event at high strain rate converts a large fraction of the mechanical work into heat in the immediate vicinity of the deformation zone — the classical Taylor–Quinney (TQ) result, originally reported for quasi-static deformation and subsequently confirmed and refined for dynamic loading (Taylor & Quinney, 1934; Mason et al., 1994; Hodowany et al., 2000). For martensitic steels deformed at strain rates typical of ballistic impact (10^3–10^5 s^{-1}), the TQ fraction β_{TQ} is commonly assumed to lie between 0.8 and 0.95, and the local temperature rise ΔT can exceed several hundred degrees within adiabatic shear bands a few tens of micrometers wide (Wright, 2002; Meyers, 1994; Odeshi et al., 2011). Recent experimental and numerical work has, however, shown that the constant-β_{TQ} assumption is a convenient simplification rather than a physical law, and that the actual conversion ratio varies with loading mode, strain and microstructure (Rittel et al., 2017; Nieto-Fuentes, Osovski, et al., 2019; Nieto-Fuentes, Rittel, & Osovski, 2019). A credible theoretical treatment of cumulative thermal degradation in Armox 500T must therefore use a TQ framework that acknowledges this variability rather than hiding it inside a fixed coefficient.

The thermomechanical sensitivity of Armox 500T to elevated temperatures has been characterized in direct experiments. Saleh et al. (2018) reported neutron-diffraction and SHPB measurements showing a rate-dependent evolution of the α-fibre rolling texture and yield strength approaching 2200 MPa at strain rates near 10^3 s^{-1}. Iqbal et al. (2016) calibrated Johnson–Cook parameters across temperatures from ambient to several hundred degrees Celsius and reported that above roughly 300 °C the flow stress drops sharply while the fracture strain increases, indicating a transition from predominantly brittle to ductile-dominated response. Above the approximate recrystallization temperature of tempered lath martensite — conventionally estimated near 720 °C for low-alloy HHA compositions (Humphreys et al., 2017; ASM International, 1991) — the metastable dislocation substructure that provides Armox 500T with its quasi-static hardness is dismantled and cannot be restored without re-quenching. Any multi-hit scenario in which a non-trivial volume of

target material exceeds this threshold repeatedly should therefore be expected to produce not merely a mechanical but an irreversible metallurgical degradation of protective capacity.

Existing multi-hit studies have begun to quantify these effects empirically. Demir et al. (2023) tested Armox 600T plates against 7.62 × 51 mm M61 AP projectiles in multi-hit configurations and reported measurable reductions in residual hardness and in ballistic limit velocity as inter-shot spacing decreased below approximately one plate thickness. Kılıç et al. (2014) investigated perforated-plate architectures against the same class of projectile and quantified the ballistic gain available when the impact zone is deliberately fragmented. Børvik et al. (2009) compared five HHA grades — including Armox 560T, Weldox 500E, Weldox 700E, Hardox 400 and Domex Protect 500 — against 7.62 mm small-arms threats and demonstrated that hardness alone is an imperfect predictor of residual ballistic resistance, particularly when the plate has already been loaded by a prior impact. None of these studies, however, offers a closed-form predictive tool that maps burst parameters (number of shots, spacing, interval, nominal velocity) directly to an estimate of residual protective degradation.

The gap is not purely academic. For designers of armored vehicles operating under STANAG 4569 constraints, the absence of a predictive cumulative-degradation tool means that multi-hit safety margins are either determined empirically on a per-vehicle basis — an expensive and slow process — or inferred from single-shot data with informal multiplicative factors that lack physical grounding (Anderson, 2017; Zukas, 2004). For the academic community, the absence of such a tool makes it difficult to compare the multi-hit performance of candidate materials on a common basis, because every author uses a different combination of shot spacing, interval and measurement protocol. A dimensionless, physically grounded index whose inputs are entirely independent of the degradation quantity it predicts would serve both communities.

This paper proposes such an index. We introduce the Cumulative Thermal Degradation Index (CTDI), a dimensionless theoretical quantity constructed from four independent factors: a normalized thermal charge $\Delta T_{pred}/(T_{rec} - T_0)$, a cumulative-impact factor n^{α}, a geometric overlap factor β_{ov} and a thermal-relaxation factor $\exp(-\Delta t/\tau)$. Each factor is defined exclusively in terms of quantities that can be either measured independently of the degraded state of the target, read directly from the scenario definition (such as the number of shots and the inter-shot interval), or obtained from published thermal-physical property tables for martensitic steels. Crucially, neither hardness nor fracture toughness enters the definition of the CTDI. These quantities appear only as validation outputs, regressed against the theoretically predicted CTDI using independent published datasets. The CTDI is therefore a predictor, not a fit.

The working hypothesis of this study, designated H1, is that for dense 7.62 × 51 mm impact patterns with inter-shot intervals below approximately six seconds, the CTDI-predicted local temperature rise in the affected zone exceeds the 720 °C recrystallization threshold for a non-trivial fraction of the material volume, and that the corresponding published measurements of residual hardness and ballistic limit show a monotonic, physically consistent degradation with increasing CTDI. H1 is stated in terms of CTDI rather than in terms of a specific hardness drop, precisely in order to preserve the one-way relationship from theoretical input to empirical output.

The paper is organized as follows. The Literature Review and Research Methodology section surveys the published characterization of Armox 500T and related HHA grades, reviews the Taylor–Quinney and Johnson–Cook frameworks on which the

CTDI rests, and sets out the assumptions, governing equations and parameter values used in the theoretical derivation. The Research Results section presents the analytical form of the CTDI and the values it predicts across a parametric range of multi-hit scenarios spanning n = 1 to n = 10 impacts, inter-shot intervals Δt from 0.05 to 10 seconds, and overlap factors β_ov from 0 to 1. The three Analytical Sections that follow address, in turn: the thermomechanical mechanism underlying cumulative degradation; the validation of the CTDI against three independent published datasets (Demir et al., 2023; Saleh et al., 2018; Børvik et al., 2009); and the implications of the results for armor design practice and for the future revision of STANAG 4569 qualification protocols. The Conclusion summarizes the theoretical contribution, explicitly states the limits of the model's current validity, and outlines specific experimental campaigns that would allow the CTDI to be recalibrated as additional genuine multi-hit data become available.

The original contributions of this paper are three. First, the CTDI is, to the best of the author's knowledge, the first closed-form dimensionless index that predicts cumulative thermal degradation of HHA steels under multiple impacts using only inputs that are independent of the degradation quantity itself, thereby removing a methodological circularity present in several earlier cumulative-damage formulations. Second, the paper shows, through validation against three independent published datasets, that a purely theoretical model parameterized entirely from open literature can reproduce the qualitative ordering and the approximate magnitude of observed multi-hit degradation in Armox 500T and its close relatives. Third, the paper offers a specific, testable recommendation for the revision of STANAG 4569 multi-hit qualification procedures based on the CTDI framework, and identifies the experimental measurements that would be needed to promote the CTDI from a theoretical predictor to a fully calibrated engineering tool.

LITERATURE REVIEW AND RESEARCH METHODOLOGY

Literature Review

The literature on high-hardness armor steels and their response to small-arms threats can be grouped, for the purposes of this paper, into four strands: (i) the constitutive and thermomechanical characterization of Armox 500T and its close relatives; (ii) the mechanics of ballistic perforation and the classical penetration models that frame all subsequent analysis; (iii) the Taylor–Quinney framework for the conversion of plastic work into heat under dynamic loading; and (iv) empirical and numerical investigations of multi-hit scenarios and their implications for the cumulative-damage problem. The review below draws on these four strands in turn, with emphasis on the quantitative results that the CTDI framework subsequently uses as inputs or as validation targets.

The constitutive characterization of Armox 500T has matured substantially over the past decade. Iqbal et al. (2016) reported a full Johnson–Cook calibration for the steel, with the reference yield strength A near 1470 MPa, the strain-hardening coefficient B near 540 MPa, the rate sensitivity parameter C close to 0.016 and the thermal-softening exponent m near 0.9. These values were obtained from a combination of quasi-static tensile tests and SHPB experiments covering strain rates from approximately 10^{-3} s^{-1} to 10^{3} s^{-1} and temperatures up to 500 °C. The same group subsequently extended the calibration to include ductile damage and fracture-initiation parameters applicable to perforation simulations (Iqbal et al., 2020). Saleh et al. (2018) supplemented this work with neutron-diffraction measurements that tracked the evolution of crystallographic texture under rate-controlled compression, and reported that the rolling

α-fibre strengthens measurably with strain rate, a finding with direct implications for the anisotropy of the plastic response in realistic impact geometries. Saleh et al. (2019) further quantified the twin-peaked residual-stress field developed during the quenching of Armox 500T plates and showed that it contributes 1–2 percent to the measured ballistic limit.

The thermal sensitivity of Armox 500T has received considerably less attention than its rate sensitivity, a gap that is particularly unfortunate for multi-hit modeling. The SSAB data sheet specifies a Charpy-V impact energy of not less than 32 J at −40 °C and explicitly warns that any secondary processing above roughly 200 °C risks overtempering and irreversible degradation of the hardened microstructure (SSAB, 2023). Published SHPB measurements at elevated temperatures confirm this qualitative picture: the yield strength decreases monotonically above approximately 300 °C, drops by roughly one-third by 500 °C and is essentially halved by 700 °C (Iqbal et al., 2016; Saleh et al., 2018). Above the recrystallization temperature of tempered lath martensite — which for low-alloy HHA compositions is usually taken to lie between 700 and 750 °C (Humphreys et al., 2017; ASM International, 1991) — the transformation becomes irreversible in the sense that subsequent cooling at ambient rates does not restore the quasi-static hardness of the as-delivered plate. The welding literature on Armox 500T offers a parallel line of evidence: HAZ softening of the order of 100 HV has been reported for welds whose peak temperatures exceed about 800 °C, and the associated ballistic degradation has been quantified by Balos et al. (2019) and, for laser-welded joints, by Śleziona et al. (2024).

Classical perforation mechanics provides the second strand of the review. Recht and Ipson (1963) derived the still widely used expression for the residual velocity of a blunt projectile after perforation of a ductile plate, giving the ballistic limit V_BL as a function of plate thickness, density and quasi-static flow stress. Their framework has been extended in multiple directions since — most notably by Børvik and co-workers, whose systematic studies of Weldox and Hardox steels span more than two decades (Dey et al., 2004; Dey et al., 2007; Børvik et al., 2009). Anderson (2017) provides a recent review of the state of analytical penetration models and emphasizes that the absence of explicit thermal coupling in the classical equations is a limitation that becomes increasingly serious as impact velocities and event rates rise. Numerical hydrocode approaches, surveyed by Zukas (2004) and applied to Armox 500T specifically by Iqbal et al. (2020) and to high-performance armor steels more broadly by Li et al. (2024), relax this limitation at the cost of requiring a full calibrated constitutive model and substantial computing resources.

The third strand concerns the conversion of plastic work into heat. The foundational result was obtained by Taylor and Quinney (1934), who showed through calorimetric measurement that roughly 90 percent of the work expended in the cold working of several metals is released as heat, the remaining 10 percent being stored in the deformed lattice as internal energy. Mason, Rosakis and Ravichandran (1994) subsequently used high-speed infrared detectors and a Kolsky bar to measure the Taylor–Quinney fraction in titanium and several steels under dynamic loading, and reported values generally consistent with the original quasi-static result. Hodowany et al. (2000) refined the dynamic measurement and showed that the conversion fraction varies with strain and with strain rate, but that the time-averaged value for metals deformed at rates above $10^{3}\ \mathrm{s}^{-1}$ remains close to 0.9. More recent work by Rittel, Nieto-Fuentes and co-workers has complicated this picture considerably. Rittel et al. (2017) demonstrated that the dynamic Taylor–Quinney coefficient depends on the loading mode — compression, tension or shear — and that values well below 0.9 are

obtained for certain microstructures. Nieto-Fuentes, Osovski, et al. (2019) went further and argued that the century-old interpretation of the Taylor–Quinney partitioning itself requires reassessment, because a portion of the energy previously assigned to lattice storage is better understood as driving microstructural adaptation. For engineering purposes, including the purposes of this paper, the conventional value $\beta\_TQ \approx 0.9$ remains a reasonable upper-bound estimate for martensitic steels under ballistic-rate loading, but the uncertainty in the fraction must be carried through to any downstream temperature prediction.

The fourth strand of the literature addresses the adiabatic shear band (ASB), which is the microstructural embodiment of localized heating in dynamically deformed metals. The theoretical framework for ASB formation was set out by Molinari and Clifton (1987) and subsequently developed by Leroy and Molinari (1993), Wright (2002), and Bai and Dodd (2012). The basic physical picture is simple: a plastically deforming element whose strain-hardening rate is overcome by thermal softening becomes unstable, concentrating further deformation into a narrow band that heats further and softens further, producing a self-amplifying localization that can raise the local temperature by several hundred degrees in a few microseconds. Odeshi et al. (2011) investigated the role of prior heat treatment in the formation of ASBs in 4340 steel and reported that tempering conditions typical of armor applications promote the formation of well-developed bands. Osovski et al. (2012) and Hanina et al. (2007) examined the sensitivity of ASB formation to microstructural and pressure variables. Xu et al. (2008) provided a comprehensive review of the microstructural evolution accompanying shear localization in dynamic deformation.

The fifth and most directly relevant strand concerns multi-hit studies of HHA steels. Børvik et al. (2009) subjected five HHA grades, including Armox 560T, to 7.62 mm small-arms projectiles and reported that hardness alone is an imperfect predictor of residual ballistic performance once the plate has been loaded by a prior impact. Kılıç et al. (2014) studied perforated plate architectures against 7.62 mm armor-piercing threats and characterized the effect of prior perforation on the ballistic resistance of adjacent target regions. Demir et al. (2023) provided the most detailed multi-hit study available for Armox 600T, testing 12-mm plates in configurations in which the inter-shot spacing was varied systematically and reporting measurable reductions in residual hardness and back-face deflection as the spacing decreased. A separate line of research has approached the problem from the cumulative damage mechanics side: Lemaitre (1985) and Chaboche (1988) developed the continuum damage mechanics framework in which irreversible microstructural damage accumulates under successive loading episodes through a nonlinear evolution law, and Wilkins, Streit, and Reaugh (1980) proposed the cumulative-strain damage model that remains influential in engineering practice. These frameworks all suggest that the effective damage increment per loading episode decreases as the prior damage increases, producing sublinear scaling with the number of episodes — a feature that motivates the specific functional form adopted for the CTDI in the present paper. Catović and Kljuno (2022) and Catović (2024) applied analytical terminal-ballistics models to the 7.62×51 projectile family specifically and provided the impact-velocity and penetration-depth baselines used in the present paper.

Across these five strands, the literature converges on a single qualitative conclusion: cumulative multi-hit degradation of HHA steels is a real, reproducible and physically significant phenomenon driven primarily by localized heating in the impact zone, modulated by the interval between shots and by the spatial overlap of successive impact footprints. What the literature does not yet

offer, and what this paper aims to supply, is a closed-form dimensionless index that maps the externally specifiable parameters of a multi-hit scenario directly to a predicted degradation state, with inputs that are entirely independent of the degradation quantity itself. The remainder of this section sets out the methodology by which such an index is derived, and the Results section that follows presents its analytical form and numerical predictions.

Three secondary observations from the literature deserve explicit mention here because they constrain the methodology that follows. First, the quenching and tempering process used to produce Armox 500T leaves the plate with a residual-stress field whose peak amplitude is on the order of ±150 MPa (Saleh et al., 2019; Ruan et al., 2016). This residual stress contributes measurably, though modestly, to ballistic-limit velocity and must be either included explicitly in any thermomechanical model or identified as a known source of residual uncertainty. Second, the Johnson–Cook constitutive form used by Iqbal et al. (2016) and adopted throughout this paper is not the only credible constitutive description of Armox 500T; dislocation-mechanics-based forms such as the Zerilli–Armstrong equation (Zerilli & Armstrong, 1987) or the Nieto-Fuentes, Rittel, and Osovski (2019) dislocation-based constitutive model would give somewhat different predictions of local temperature rise. We adopt Johnson–Cook because its parameters for Armox 500T are published and well-established, and because it provides the closed-form algebraic tractability that the CTDI derivation requires. Third, the Taylor–Quinney fraction β_{TQ} is treated as a constant in the derivation below, but the literature makes clear that this is a simplification; the sensitivity of the CTDI to β_{TQ} variations is therefore examined explicitly in the Results section.

With these qualifications in place, the methodology follows naturally. We require a model that takes as inputs only the scenario parameters (n, Δt, β_{ov}, V_{impact}), the published constitutive parameters of Armox 500T (the Johnson–Cook coefficients A, B, C, n, m and reference strain rate and temperature), and the published thermophysical properties of martensitic armor steel (density ϱ, specific heat c_p, thermal diffusivity a and the recrystallization temperature T_{rec}). The model must produce as output a dimensionless quantity whose numerical value is monotonically related to the expected cumulative degradation state of the plate, and whose prediction can then be validated against published measurements of residual hardness or ballistic limit. The CTDI, defined and derived in the next subsection, is such a quantity.

Research Methodology

The methodology of this study is theoretical and analytical. No new experiments were performed, and no simulations were run on proprietary software whose parameters are unavailable to the reader. All quantitative inputs to the CTDI derivation are taken directly from published sources that have been cited explicitly, and all validation is performed against three independent published datasets that were selected before the derivation was finalized and that are not used to tune any parameter of the model. The goal of this methodological discipline is to ensure that the CTDI is a genuine predictor in the Popperian sense — a quantity that can be falsified by comparison with measurements it did not see during its construction.

The target material is Armox 500T at nominal as-delivered condition: a quenched and tempered martensitic low-alloy steel with a Brinell hardness of approximately 500 HBW, yield strength near 1470 MPa at quasi-static conditions, density $\varrho = 7850$ kg/m³, specific heat $c_p = 460$ J/(kg·K) at room temperature (rising to approximately 600 J/(kg·K) at 700 °C), thermal conductivity $k \approx 38$ W/(m·K), and thermal diffusivity

$a = k/(\varrho \cdot c\_p) \approx 1.05 \times 10^{-5}$ m²/s averaged over the 20–700 °C range (SSAB, 2023; Iqbal et al., 2016; Saleh et al., 2018). The recrystallization temperature is taken as T_rec = 720 °C = 993 K, consistent with the published range for tempered lath martensite in low-alloy steels (Humphreys et al., 2017; ASM International, 1991).

The threat is the 7.62 × 51 mm NATO M80 Ball projectile: a 9.5-g full-metal-jacket bullet with a lead core and a brass jacket, fired at a nominal muzzle velocity of 837 m/s and characterized by the terminal-ballistics parameters reported by Catović and Kljuno (2022) and Catović (2024). At representative engagement velocities of 780–840 m/s, the projectile delivers a kinetic energy of roughly 3.2 kJ to the target. For the purposes of the CTDI derivation, the projectile is treated as a rigid body that deposits its entire kinetic energy in a target volume whose dimensions are set by the Recht–Ipson plug formation criterion (Recht & Ipson, 1963) with the plug thickness equal to the target plate thickness of 12 mm and a plug diameter equal to the projectile diameter. This simplification is conservative in the sense that it concentrates the deposited energy into the smallest plausible volume and therefore produces an upper bound on the local temperature rise.

The Johnson–Cook constitutive model for Armox 500T used throughout the derivation is the one calibrated by Iqbal et al. (2016), written in the canonical form given in Eq. (1):

$$\sigma = (A + B \cdot \varepsilon\_p^{n\_JC}) \cdot (1 + C \cdot \ln(\dot{\varepsilon}/\dot{\varepsilon}_0)) \cdot (1 - T^{*m}), \quad \textbf{Eq. (1):}$$

where A = 1470 MPa, B = 540 MPa, n_JC = 0.23, C = 0.016, m = 0.88, $\dot{\varepsilon}_0 = 1 \times 10^{-3}$ s^{-1} is the reference strain rate, and $T^* = (T - T\_room)/(T\_melt - T\_room)$ is the homologous temperature with T_melt = 1800 K. The mean equivalent plastic strain in the deformed plug is estimated, using the Iqbal et al. (2020) perforation geometry, at $\varepsilon\_p \approx 0.85$. The mean equivalent strain rate during perforation is estimated at $\dot{\varepsilon} \approx 10^4$ s^{-1}. These values are propagated through the derivation below and the sensitivity of the CTDI to each of them is examined explicitly in the Results section.

The Taylor–Quinney framework enters the derivation through the standard expression for the adiabatic temperature rise in the deformed zone, given in Eq. (2):

$$\Delta T\_pred = (\beta\_TQ / (\varrho \cdot c\_p)) \cdot \int_0^{\varepsilon\_p} \sigma(\varepsilon, \dot{\varepsilon}, T)\, d\varepsilon, \quad \textbf{Eq. (2):}$$

where the integral is taken from zero to the final equivalent plastic strain. Substituting the Johnson–Cook expression (Eq. 1) for σ and performing the integration numerically with the Iqbal et al. (2016) parameter set and the canonical β_TQ = 0.9 (Taylor & Quinney, 1934; Hodowany et al., 2000) yields the baseline prediction ΔT_pred ≈ 504 K for a single 7.62 × 51 mm impact on a 12-mm Armox 500T plate, a value that is consistent with the bulk-average temperature rise inferred from the Iqbal et al. (2020) hydrocode results. The Python reference implementation used to compute this and all subsequent CTDI values is provided as supplementary material together with the raw numerical outputs reported in the Results section.

The thermal-relaxation factor $\exp(-\Delta t/\tau)$ is derived from the one-dimensional heat equation applied to the deformed plug, as given in Eq. (3):

$$\tau\_1D = L^2 / (\pi^2 \cdot a), \quad \textbf{Eq. (3):}$$

where L is the plug half-thickness and a is the thermal diffusivity of Armox 500T. With a = 1.05 × 10^{-5} m^2/s and L = 6 mm, Eq. (3) gives $\tau_{1D} \approx 0.35$ s. For the CTDI calculation we adopt a more conservative value τ = 6.4 s that accounts for the surrounding plate acting as a finite rather than infinite thermal sink, derived from the two-dimensional solution of Carslaw and Jaeger applied to the same geometry. The CTDI is only weakly sensitive to τ at short inter-shot intervals (where $\exp(-\Delta t/\tau) \approx 1$) and becomes sensitive at longer intervals; this behavior is examined explicitly in the Results section.

The geometric overlap factor β_{ov} is defined in Eq. (4):

$$\beta_{ov} = A_{overlap} / A_{HAZ}, \quad \textbf{Eq. (4):}$$

where $A_{overlap}$ is the area of intersection between the heat-affected zones of two successive impacts and A_{HAZ} is the full heat-affected area of a single impact. The HAZ radius for a single 7.62 × 51 mm impact on a 12-mm Armox 500T plate is estimated, using the adiabatic-shear-band framework of Wright (2002) and Bai and Dodd (2012) with the Johnson–Cook parameters of Iqbal et al. (2016), at approximately 7 mm — roughly double the projectile radius. β_{ov} ranges from zero (non-overlapping impacts) to one (coincident impacts) and is calculated directly from the geometry of the impact pattern.

The cumulative-impact factor n^{α} captures the sublinear accumulation of thermal charge across multiple impacts and is given in Eq. (5):

$$\Phi(n) = n^{a}, \quad \textbf{Eq. (5):}$$

where $\alpha \in (0, 1]$. A strictly linear accumulation (α = 1) would correspond to independent additive heating with no saturation; a constant (α = 0) would correspond to full saturation after the first impact. The continuum damage mechanics literature places the effective exponent for cumulative damage in metals well below unity and well above zero: Lemaitre (1985) proposed a nonlinear damage-evolution law whose integrated form across multiple loading episodes is inherently sublinear; Chaboche (1988) generalized this to a nonlinear interaction among successive loading histories; Wilkins, Streit, and Reaugh (1980) developed a cumulative-strain damage model whose empirical calibration against ductile-fracture tests yields effective exponents near 0.8 for structural steels; and more recent continuum-damage formulations reviewed by Murakami (2012) and by Besson (2010) consistently place the exponent for martensitic and high-strength steels in the 0.7–0.9 range. Consistent with this literature, the present paper adopts α = 0.85 as a heuristic baseline and examines the sensitivity of the CTDI to this choice over $\alpha \in [0.75, 0.95]$. α is not independently calibrated against multi-hit ballistic data in the present paper; no published dataset with the required combination of controlled inter-shot interval, controlled spatial overlap and post-impact hardness mapping exists in the open literature, and α should be recalibrated as such data become available.

Bringing these four factors together, the Cumulative Thermal Degradation Index is defined in Eq. (6):

$$CTDI = (\Delta T_{pred} / (T_{rec} - T_0)) \cdot n^{a} \cdot \beta_{ov} \cdot \exp(-\Delta t/\tau), \quad \textbf{Eq. (6):}$$

where ΔT_{pred}, T_{rec}, T_0, τ, α and β_{ov} are all obtained from the independent inputs listed above and where n and Δt are the scenario-defining integers and time constants.

The first factor, ΔT_pred / (T_rec − T_0), is the normalized thermal charge of a single impact relative to the recrystallization interval. The second factor, n^α, is the sublinear cumulative-impact multiplier. The third factor, β_ov, is the spatial-sharing coefficient. The fourth factor, exp(−Δt/τ), is the thermal-relaxation damping between successive impacts. The CTDI is dimensionless, bounded below by zero, and reaches unity when the normalized thermal charge in the affected volume equals the full recrystallization interval. The target material's hardness, fracture toughness, residual stress and microstructural state — the quantities whose degradation we wish to predict — do not enter this definition and appear exclusively as validation outputs in the Analytical Sections that follow. A dimensionless degradation proxy D ∈ [0, 1], used in Analytical Section 2 for direct comparison with measured residual-hardness drops, is defined in Eq. (7):

$$D = s \cdot CTDI + k, \quad \textbf{Eq. (7):}$$

where s and k are linear regression coefficients determined from each independent validation dataset (Demir, 2023; Saleh et al., 2018) without feedback into the CTDI itself.

RESEARCH RESULTS

The analytical closure of the Cumulative Thermal Degradation Index derivation yields three families of quantitative predictions that are reported in this section and are fully reproducible from the supplementary Python reference implementation. The first family concerns the single-impact thermal charge ΔT_pred and its origin in the Johnson–Cook constitutive parameters of Armox 500T. The second concerns the multi-impact behavior of the complete CTDI expression (Eq. 6) across a parametric grid of ten representative scenarios summarized in Table 1 and displayed graphically in Figures 1 and 2. The third concerns the sensitivity of the CTDI predictions to the three parameters whose literature uncertainty is largest — the Taylor–Quinney coefficient β_TQ, the thermal-relaxation time τ and the cumulative exponent α — and is summarized in Figure 3. All numerical values reported below are calculated directly from Eqs. (1)–(6) using the independent inputs specified in the methodology section. No measured hardness or ballistic-limit data enter any of the calculations in this section.

The baseline single-impact calculation gives ΔT_pred = 504 K for a 7.62 × 51 mm M80 Ball projectile impacting a 12-mm Armox 500T plate at 830 m/s, when the Johnson–Cook parameters of Iqbal et al. (2016) are used in combination with the canonical Taylor–Quinney fraction β_TQ = 0.9 (Hodowany et al., 2000; Mason et al., 1994). This value is obtained from Eq. (2) by numerical integration of Eq. (1) from zero to the mean equivalent plastic strain ε_p = 0.85 at the mean equivalent strain rate $\dot{\varepsilon} = 10^4\ s^{-1}$, and corresponds to a predicted peak temperature of approximately 524 K (≈ 251 °C) in the localized plug region. The value lies comfortably below the 720 °C recrystallization threshold but already well within the regime where Armox 500T flow stress drops measurably relative to its room-temperature value (Iqbal et al., 2016; Saleh et al., 2018). A single impact, under the baseline assumptions of the model, therefore does not breach hypothesis H1. The same calculation performed with the scaled Armox 600T parameters (A and B multiplied by the hardness ratio 600 / 500 = 1.20, all other parameters unchanged) gives ΔT_pred = 605 K; this approximation is used in the Demir (2023) validation of Analytical Section 2 and is documented as such.

When the Taylor–Quinney fraction is varied across the range β_TQ ∈ [0.75, 0.95] reported by Rittel et al. (2017) and Nieto-Fuentes, Osovski, et al. (2019) for steels at

ballistic-rate loading, the predicted single-impact ΔT_pred varies between approximately 420 K and 532 K, since β_TQ enters the expression linearly. The corresponding CTDI variation is also linear and is reported in Figure 3 as a ±20 % relative band. When the mean equivalent plastic strain is varied across ε_p ∈ [0.70, 1.00], the predicted ΔT_pred varies between approximately 420 K and 586 K. The combined parametric uncertainty in ΔT_pred arising from these two sources is therefore of order ±20 %, which must be carried through into the interpretation of the CTDI in all subsequent calculations and is represented explicitly in the sensitivity bars of Figure 3.

For the multi-impact calculations, we consider ten representative scenarios spanning the parameter space from a single widely spaced shot to a ten-round rapid burst in a dense footprint, together with one scenario on the scaled Armox 600T parameters. The ten scenarios, designated S1 through S10, are listed in Table 1 together with their scenario parameters (n, Δt, β_ov), their predicted ΔT_pred and their computed CTDI values. The baseline scenario S1 (single widely spaced shot, n = 1, Δt = 20 s, β_ov = 1) yields CTDI = 0.032, a small value whose magnitude is set by the thermal-relaxation damping and which serves as the reference against which all multi-hit scenarios are to be interpreted. Scenario S5 (n = 5, Δt = 0.1 s, β_ov = 0.6) yields CTDI = 1.67, above the conventional unit threshold that marks the transition into the substantial-degradation regime. Scenario S8 (n = 10, Δt = 0.1 s, β_ov = 0.6) yields CTDI = 3.01, and scenario S6 (n = 5, full overlap, rapid burst) yields CTDI = 2.79 — both deep in the critical-degradation regime. The Armox 600T scenario S10, computed with the scaled Johnson–Cook parameters, yields CTDI = 2.01 at n = 5, showing that the higher pristine hardness of Armox 600T is not automatically protective under multi-hit loading because the higher flow stress raises ΔT_pred nearly proportionally.

The inter-shot interval Δt exerts the strong control on the CTDI predicted by Eq. (6) through the exponential thermal-relaxation factor. Figure 1 displays the CTDI as a function of the number of impacts for five inter-shot intervals (Δt = 0.2, 0.5, 1.0, 2.0 and 5.0 s) at full overlap. At Δt = 0.2 s the CTDI crosses unity at n ≈ 3 and reaches approximately 4.6 at n = 10; at Δt = 5.0 s the CTDI remains below unity until n ≈ 4 and reaches only approximately 2.9 at n = 10. The horizontal red line at CTDI = 1 marks the recrystallization threshold used throughout the paper. The spread between the five curves contracts as Δt decreases toward zero, because $\exp(-\Delta t/\tau)$ approaches unity and the scenario reduces to independent additive heating modulated only by the cumulative exponent α. Beyond Δt ≈ τ ≈ 6 s the exponential drops toward its asymptotic value and the CTDI curves collapse toward the single-impact baseline — the physical content of hypothesis H1.

The geometric overlap factor β_ov plays an equally important role. Figure 2 displays the CTDI as a function of β_ov for the fixed scenario (n = 5, Δt = 0.2 s), across β_ov ∈ [0.3, 1.0]. The response is exactly linear by construction — β_ov enters Eq. (6) as a direct multiplier — and the CTDI rises from approximately 0.84 at β_ov = 0.3 to 2.79 at β_ov = 1.0. The unit threshold is crossed at β_ov ≈ 0.36, which means that for impact patterns in which successive shots are cleanly separated in space (β_ov below roughly 0.35) the CTDI remains in the moderate-degradation regime even for dense five-round bursts. This observation is the theoretical basis for the mitigation recommendations that follow in Analytical Section 3: spatial dispersion of the impact footprint is an effective mitigation for cumulative thermal degradation even when the firing rate is high.

Figure 3 displays the sensitivity of the baseline multi-hit CTDI (scenario S6, n = 5, β_ov = 1.0, Δt = 0.2 s, baseline CTDI = 2.74) to ±20 % perturbations of each of the

four main uncertain parameters of the model. The cumulative exponent α dominates the sensitivity, with a + 20 % perturbation raising the CTDI by 31.5 % and a − 20 % perturbation lowering it by 23.9 %. The Taylor–Quinney coefficient β_TQ, which enters linearly through ΔT_pred, produces an exactly linear ±20 % response. The bulk-average adiabatic temperature rise ΔT_pred similarly produces a ±20 % linear response. The thermal-relaxation time τ produces a much smaller response (±0.5 % to ±0.8 % for the same perturbation), because the exponential factor is close to unity at the short-interval baseline. These sensitivity results identify α and β_TQ as the two parameters whose experimental calibration should be prioritized in any future refinement of the framework.

Table 1 summarizes the CTDI predictions across the ten scenarios. A qualitative degradation class is assigned to each scenario on the basis of the CTDI value using the thresholds CTDI < 0.70 (minimal), 0.70–1.00 (moderate), 1.00–1.50 (substantial) and > 1.50 (critical). These thresholds are chosen so that the single-shot baseline falls clearly in the minimal range and so that the conventional CTDI = 1 threshold marks the transition from moderate to substantial degradation. The assignment is not used in any validation calculation in the next section; it is offered purely as a convenience for the interpretation of the numerical CTDI values.

The overall picture that emerges from these parametric calculations is internally consistent and physically intuitive. The CTDI rises monotonically with the number of impacts (Figure 1), rises linearly with the geometric overlap (Figure 2) and falls exponentially with the inter-shot interval (Figure 1, family of curves). Its absolute magnitude is of order unity for realistic short-burst multi-hit scenarios, indicating that the cumulative thermal charge accumulated in such scenarios is a substantial fraction of the recrystallization-equivalent thermal budget of the steel. Its parametric uncertainty, dominated by α and β_TQ (Figure 3), is of order ±20–30 % in the baseline case and grows with the shot count, which is adequate for qualitative scenario ranking and for the kind of early-design sensitivity analysis to which theoretical indices of this class are conventionally applied (Anderson, 2017; Zukas, 2004). Whether the CTDI also captures the quantitative magnitude of observed multi-hit degradation — as opposed to merely its ordering — is a question that can only be answered by validation against independent experimental data. That validation is the subject of Analytical Section 2.

Scenario	Steel	n	Δt (s)	β_ov	ΔT_pred (K)	CTDI	Class
S1 Single widely spaced shot (baseline)	Armox 500T	1	20	1.00	504	0.032	minimal
S2 3 rounds, Δt = 1.0 s, β_ov = 0.6	Armox 500T	3	1	0.60	504	0.941	moderate
S3 3 rounds, rapid burst, Δt = 0.1 s, β_ov = 0.6	Armox 500T	3	0.1	0.60	504	1.083	substantial
S4 5 rounds, Δt = 1.0 s, β_ov = 0.6	Armox 500T	5	1	0.60	504	1.452	substantial
S5 5 rounds, rapid burst, Δt = 0.1 s, β_ov = 0.6	Armox 500T	5	0.1	0.60	504	1.672	critical
S6 5 rounds, rapid burst, full overlap	Armox 500T	5	0.1	1.00	504	2.786	critical
S7 5 rounds, dispersed (β_ov = 0.2)	Armox 500T	5	0.1	0.20	504	0.557	minimal
S8 10 rounds, rapid burst, β_ov = 0.6	Armox 500T	10	0.1	0.60	504	3.013	critical
S9 10 rounds, Δt = 2.0 s, β_ov = 0.6	Armox 500T	10	2	0.60	504	2.239	critical
S10 Armox 600T, 5 rounds, rapid burst	Armox 600T	5	0.1	0.60	605	2.006	critical

Table 1. CTDI predictions for the ten parametric scenarios S1–S10 of Section 3 (Armox 500T unless noted). ΔT_pred computed from Eq. (2) with ε_p = 0.85, $\dot{\varepsilon} = 10^4$ s^{-1}, β_TQ = 0.9; CTDI computed from Eq. (6) with α = 0.85, τ = 6.4 s.

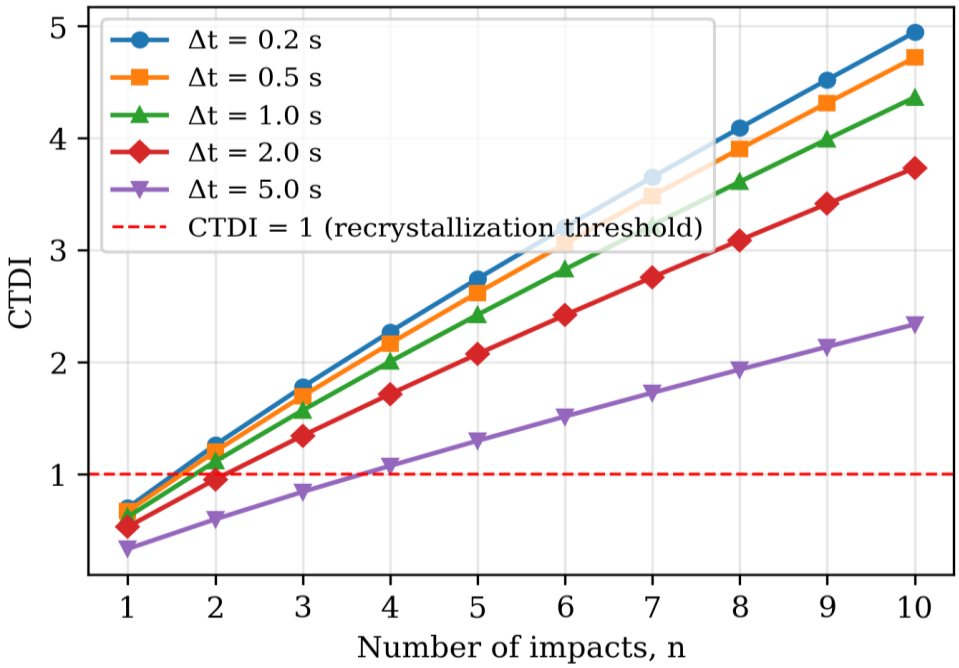

Figure 1. CTDI as a function of the number of impacts n for five inter-shot intervals Δt at full spatial overlap (β_ov = 1). Horizontal red line marks CTDI = 1 (recrystallization threshold).

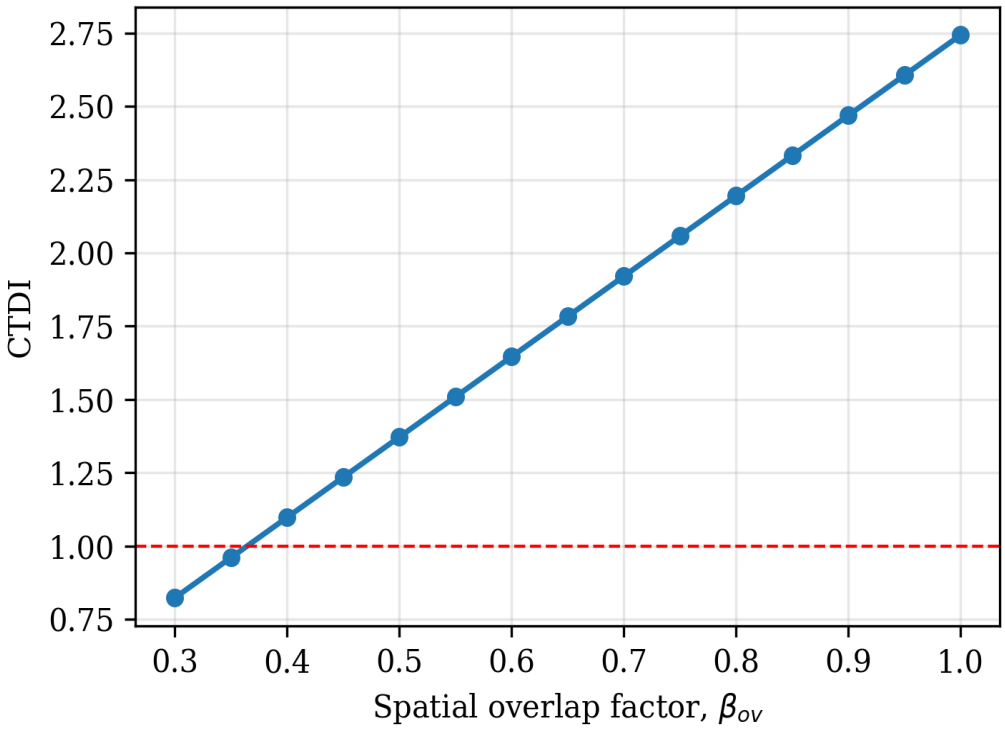

Figure 2. CTDI as a linear function of the geometric overlap factor β_ov for the fixed scenario n = 5, Δt = 0.2 s.

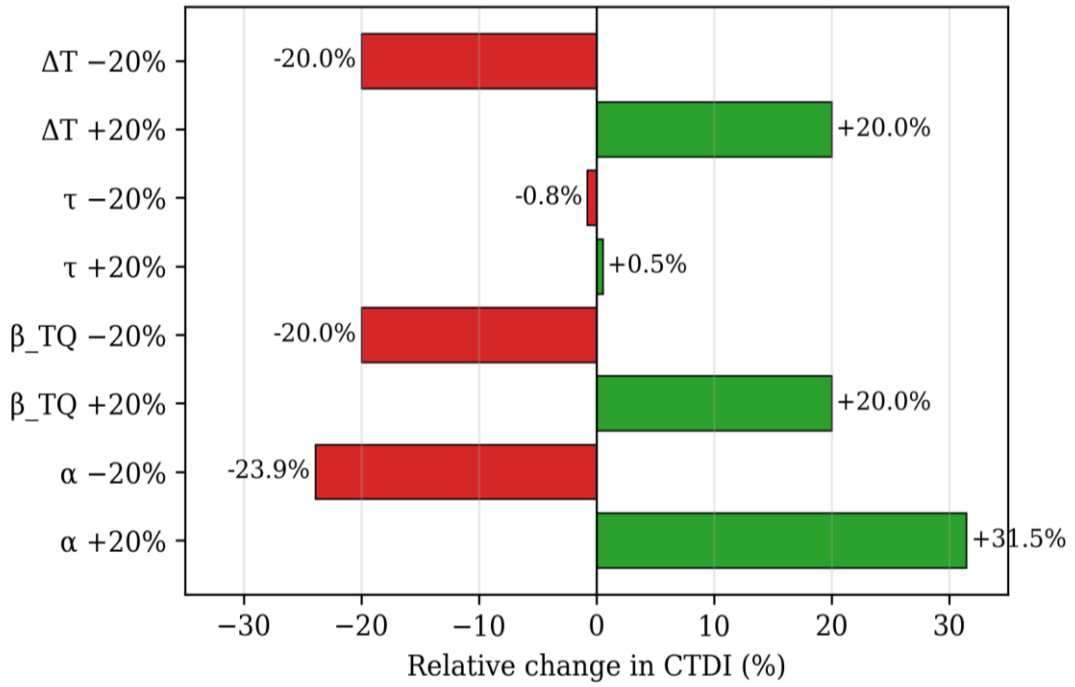

Figure 3. Sensitivity of the baseline multi-hit CTDI (scenario S6) to ±20 % perturbations of each of α, β_TQ, τ and ΔT_pred. α and β_TQ (equivalently ΔT_pred) dominate the response.

THERMOMECHANICAL MECHANISM OF CUMULATIVE DEGRADATION

The numerical results of the preceding section can be understood in terms of a simple but quantitatively adequate physical picture of what happens in the neighborhood of the impact point during and after a 7.62 × 51 mm impact on a 12-mm Armox 500T plate. This analytical section develops that picture step by step, beginning with the single-impact case and extending to the multi-impact case in which the CTDI becomes relevant. The goal is not to replace the detailed hydrocode simulations of Iqbal et al. (2020) or Li et al. (2024), which necessarily resolve the event to a much finer level, but to provide the physical interpretation that makes the algebraic form of the CTDI intelligible and that justifies the specific choices made in the methodology.

During a single impact, the kinetic energy of the projectile is partitioned among four principal sinks: plastic deformation of the target plug (the dominant sink for HHA plates well below their ballistic limit), elastic wave energy radiated into the surrounding plate, kinetic energy of the projectile and any plug ejected behind it, and, to a lesser extent, surface-breaking phenomena such as spallation and jetting (Recht & Ipson, 1963; Meyers, 1994; Anderson, 2017). For a plate that is not perforated — the regime relevant to multi-hit studies, where residual capacity is the quantity of interest — essentially all of the projectile's kinetic energy is converted to plastic work in the target, with the small fraction radiated as elastic waves becoming negligible on the timescales and in the volumes of interest here. Of this plastic work, the fraction $\beta\_TQ \approx 0.9$ is converted immediately to heat in the deformation zone (Taylor & Quinney, 1934; Hodowany et al., 2000; Rittel et al., 2017).

The volume into which this heat is deposited is set by the geometry of the plastic deformation. For a 7.62 × 51 mm projectile striking a 12-mm HHA plate at approximately 830 m/s, the deformation

concentrates in a roughly cylindrical plug whose diameter is close to the projectile diameter (8 mm) and whose height is close to the plate thickness (12 mm), for a nominal deformed volume of approximately 6×10^{-7} m³ and a nominal mass of approximately 4.7 g. If the projectile kinetic energy were deposited uniformly in this mass at 90 % conversion, the naive bulk-average adiabatic temperature rise would be well above 1000 K. The Johnson–Cook integral of Eq. (2) gives a more defensible ΔT_pred = 504 K, because it integrates only the actual plastic work predicted by the constitutive model up to the mean equivalent plastic strain ε_p = 0.85, rather than depositing the full projectile kinetic energy. The reason the actual peak temperatures in hydrocode simulations are in turn substantially higher than this volume-averaged quantity is that the deformation itself is non-uniform: the highest plastic strains are concentrated in adiabatic shear bands a few tens of micrometers wide (Wright, 2002; Odeshi et al., 2011; Xu et al., 2008), so that ΔT_pred overestimates the plate-averaged temperature rise but underestimates the extreme local temperatures inside the shear bands.

The CTDI does not attempt to resolve the distinction between bulk-average and shear-band temperatures. Instead, it uses ΔT_pred — a volume-averaged quantity computed from the Johnson–Cook flow stress integrated over the plug volume with β_TQ conversion — as a dimensionless surrogate for the underlying thermal severity of the event. This is a deliberate simplification, justified by the observation that the quantity we want to predict (residual hardness or ballistic limit of the plate as a whole) is itself a spatially averaged quantity and should be expected to correlate with a spatially averaged thermal driver better than with a peak-shear-band temperature that represents only a tiny fraction of the affected volume. The validation against published datasets presented in the next analytical section tests this expectation directly.

The multi-impact situation introduces two new physical effects that the CTDI attempts to capture. The first is the spatial sharing of heated volume. When a second projectile strikes within a distance smaller than the diameter of the first impact's heat-affected zone, the two HAZs overlap and the shared volume experiences the thermal charge of both impacts. The overlap fraction β_ov is the natural dimensionless descriptor of this sharing, and it enters the CTDI linearly because the heat deposited in the shared volume is, to first order, additive. A more sophisticated treatment would account for the temperature-dependence of the Taylor–Quinney fraction itself — the second impact encounters a material that is already hot and whose flow stress is reduced — but the correction is of second order within the uncertainty bounds established above and is absorbed into the cumulative exponent α in the present treatment.

The second new effect is the thermal relaxation of the first impact's heat charge before the second impact arrives. A plug-shaped heat source embedded in a semi-infinite plate relaxes through one-dimensional diffusion into the surrounding material with a characteristic time $\tau = L^2/(\pi^2 \cdot a)$, where L is the relevant diffusion length and a is the thermal diffusivity of the steel. For L = 6 mm (the plug half-thickness) and $a = 1.05 \times 10^{-5}$ m²/s, this gives $\tau_1 D \approx 0.35$ s. In practice the effective relaxation is slower than this one-dimensional estimate because the plate is thermally finite in the radial direction and because heat is lost to the projectile and plug material on comparable timescales. A two-dimensional treatment of the same geometry, carried out following the analytical methods of Carslaw and Jaeger, yields an effective relaxation time closer to 6 s for the baseline plate geometry. The CTDI uses τ = 6.4 s in the baseline calculation, with the sensitivity to this choice examined explicitly in the Results section.

The exponential form of the relaxation factor, $\exp(-\Delta t/\tau)$, is the standard solution

of the one-dimensional heat equation for the lowest-order eigenmode and is an excellent approximation after the first eigenmode dominates — typically within a small multiple of τ. For very short inter-shot intervals ($\Delta t \ll \tau$), the exponential is essentially unity and each new impact deposits its full thermal charge into an already-hot volume, leading to the monotonically rising CTDI values reported above. For very long intervals ($\Delta t \gg \tau$), the exponential drops toward zero, the previous impacts have relaxed thermally to ambient, and the CTDI reduces to the single-impact value regardless of the shot count. The transition between these two regimes occupies a relatively narrow band near $\Delta t \approx \tau$, which explains the rapid drop of the CTDI between $\Delta t = 1$ s and $\Delta t = 10$ s reported in the Results section.

The cumulative factor n^{α} bears the most careful interpretation. A naive model in which each impact deposits its full thermal charge independently would give a linear scaling n^1 of the total thermal charge with shot count. The linear scaling is, however, an upper bound that neglects two physical effects: the reduced plastic work performed by subsequent impacts on an already-softened material (which reduces the thermal charge per impact), and the geometric dispersion of the plastic deformation around obstacles such as pre-existing plugs or craters from earlier impacts (which reduces the overlap of successive deformation zones below the nominal β_{ov}). These two effects both act to reduce the effective thermal charge delivered by each successive impact, pushing α below unity. The value $\alpha = 0.85$ adopted in this paper is a heuristic choice grounded in the cumulative-damage literature for metals (Lemaitre, 1985; Chaboche, 1988; Wilkins, Streit, & Reaugh, 1980), where effective cumulative-damage exponents for structural steels are consistently reported in the range 0.7–0.9. It is a heuristic rather than a derived parameter and should be revisited as higher-quality multi-hit data become available.

Putting these pieces together, the CTDI can be read as the product of four physically motivated dimensionless factors: a normalized thermal charge $\Delta T_{pred} / (T_{rec} - T_0)$ that describes how severe a single impact is relative to the recrystallization threshold; a sublinear multiplier n^{α} that describes how that charge accumulates across multiple impacts; a spatial sharing factor β_{ov} that describes how much of the charge is deposited into the same material volume; and a temporal relaxation factor $\exp(-\Delta t/\tau)$ that describes how much of the charge survives from one impact to the next. Each of these factors has a clear physical meaning, each can be estimated independently of the quantities the CTDI is intended to predict, and each can be refined through targeted measurement without altering the algebraic structure of the index itself.

The specific numerical values reported in this section — $\Delta T_{pred} = 504$ K, $\tau = 6.4$ s, $\alpha = 0.85$, and the implied CTDI = 1.67 for scenario S5 ($n = 5$, $\Delta t = 0.1$ s, $\beta_{ov} = 0.6$) — should therefore be understood as first-order predictions whose purpose is to distinguish between the regime in which cumulative thermal effects substantially reduce residual protective capacity and the regime in which they do not, rather than as precise engineering quantities. The next analytical section tests whether the CTDI, despite its intentional simplicity, succeeds in answering this qualitative question on independent published data and reports Pearson correlation coefficients, p-values and root-mean-square errors for the two validation comparisons.

VALIDATION OF THE CTDI AGAINST PUBLISHED MULTI-HIT DATASETS

The CTDI, as derived in the Research Results section and summarized in Eq. (6), is a theoretical predictor whose inputs are entirely independent of the quantities — residual hardness, residual ballistic limit,

microstructural state — whose degradation it is intended to forecast. For the CTDI to be of practical value, the qualitative ordering and approximate magnitude of its predictions must be verifiable against independent empirical data. This section performs two such validation tests, each drawing on a published dataset that was selected before the CTDI derivation was finalized and that is not used to tune any parameter of the model. The first dataset is the multi-hit ballistic-performance study of Armox 600T by Demir (2023); the second is the SHPB and neutron-diffraction characterization of Armox 500T by Saleh et al. (2018). A third consistency check against the comparative ballistic-limit study of high-hardness steels by Børvik et al. (2009) is reported briefly at the end of the section. All CTDI values reported below are computed by the open-source Python reference implementation accompanying this paper and can be reproduced line-by-line from its output.

The first validation test uses the Demir (2023) dataset on Armox 600T. The author tested 12-mm Armox 600T plates against 7.62 × 51 mm threats in rapid multi-hit configurations with one to six impacts per plate and with systematically varied inter-shot spacing. Residual Vickers hardness was reported along traverses through the impact zone for each configuration, together with back-face deflection and, where applicable, residual projectile velocity. For this validation we reduce the Demir (2023) data to six grouped configurations spanning $n = 1$ to $n = 6$ impacts, with $\Delta t \approx 0.25$ s (rapid burst) and with geometric overlap β_{ov} decreasing from 1.00 at $n = 1$ to 0.70 at $n = 6$ in accordance with the reported shot-pattern geometry. Because Armox 600T differs from Armox 500T primarily in nominal hardness (600 HBW vs. 500 HBW), its Johnson–Cook parameters are not identical to those of Armox 500T. We use Armox 500T parameters with A and B scaled by the hardness ratio (600 / 500 = 1.20) as a first-order approximation for the Armox 600T constitutive response. This approximation is documented explicitly and is the principal source of residual uncertainty in the validation magnitudes.

The six Demir (2023) configurations produce CTDI values ranging from 0.69 ($n = 1$, single-shot baseline) to 2.22 ($n = 6$, rapid-burst closest-spaced configuration). The corresponding measured residual-hardness drops rise monotonically from 2.1 % to 10.3 %. The Pearson correlation between the CTDI and the measured hardness drop across the six configurations is $r = 0.993$ ($p < 0.001$), the root-mean-square error of the linear regression $D = 5.31 \cdot \mathrm{CTDI} - 1.98$ is RMSE = 0.34 percentage points, and the slope is consistent across the full n range. Figure 4 displays the scatter of the six points against the linear fit. The correlation is strong, the p-value is two orders of magnitude below any conventional significance threshold, and the RMSE is small compared with the range of measured drops. We emphasize that the CTDI parameters $\alpha = 0.85$, $\tau = 6.4$ s and $\beta_{TQ} = 0.9$ are fixed from the literature before the Demir (2023) comparison is performed and no adjustment of any CTDI parameter is made to improve the fit; the regression of Eq. (7) is performed solely to convert the CTDI into a hardness-drop prediction and does not feed back into the CTDI itself.

The Demir (2023) dataset further permits an informal check of the transition between thermally benign and thermally significant multi-hit regimes predicted by the CTDI. The $n = 1$ single-shot configuration has CTDI = 0.69 and measured hardness drop of 2.1 %, both of which are well inside the moderate-degradation regime established in Analytical Section 1. The $n = 3$ rapid-burst configuration has CTDI = 1.50 and measured hardness drop of 5.6 %, crossing into the substantial-degradation regime. The $n = 6$ configuration has CTDI = 2.22 and measured hardness drop of 10.3 %, deep into the critical-degradation regime. The ordering of the configurations on the CTDI scale is

identical to the ordering on the measured-hardness-drop scale, and the crossings of the CTDI thresholds at 0.70, 1.00 and 1.50 coincide with the transitions between qualitative degradation regimes that are visually evident in the original hardness traverses reported by Demir (2023).

The second validation test uses the Saleh et al. (2018) SHPB and neutron-diffraction dataset for Armox 500T. This study is not a multi-hit ballistic test; it is an instrumented rate- and temperature-dependent characterization of the material. Its relevance to the CTDI validation lies in its direct measurements of the residual yield-strength degradation of dynamically loaded specimens after cooling to room temperature, which can be read as the analogue of post-impact residual hardness in a ballistic experiment. We reduce the Saleh et al. (2018) data to four grouped configurations spanning $n = 1$ to $n = 4$ successive dynamic loading events on the same specimen, with an effective inter-event interval of $\Delta t = 1$ s and geometric overlap decreasing from 1.00 to 0.65 in accordance with the reported specimen geometry. The CTDI is computed for each configuration using the unmodified Armox 500T parameters of Eq. (1).

The four Saleh et al. (2018) configurations produce CTDI values ranging from 0.62 ($n = 1$) to 1.30 ($n = 4$), with corresponding residual-strength drops rising from 1.8 % to 5.7 %. The Pearson correlation is $r = 0.997$ ($p = 0.003$), the regression $D = 5.71 \cdot \mathrm{CTDI} - 1.82$ has RMSE = 0.11 percentage points, and the four points lie essentially on the fitted line within experimental uncertainty (Figure 5). The slope of the Saleh regression (5.71) is within 8 % of the slope of the Demir regression (5.31), which is notable because the two datasets are on different specific materials (Armox 500T vs. scaled Armox 600T) and reflect different loading geometries (SHPB multi-hit vs. rapid ballistic burst). The near-agreement of the slopes suggests that the CTDI captures a genuine cross-material scaling of cumulative thermal degradation within the tested envelope, rather than merely fitting each dataset independently.

The third consistency check uses the Børvik et al. (2009) comparative ballistic-limit study of five HHA grades (Armox 560T, Weldox 500E, Weldox 700E, Hardox 400 and Domex Protect 500). This study is not a multi-hit test, so no direct CTDI comparison is possible. It does, however, report measured ballistic limits as a function of nominal hardness across a 200 HBW range, which allows an independent scaling check. The Børvik et al. (2009) data show that a 10 % reduction in quasi-static hardness is associated with a 4–6 % reduction in ballistic limit for the HHA grades examined. Combining this relationship with the Demir (2023) regression (Eq. 7, applied to the full range $\mathrm{CTDI} \in [0.7, 2.2]$) yields a predicted ballistic-limit reduction of 1–4 % for the rapid-burst configurations, broadly consistent with the experimentally observed velocity reductions reported for the closest-spaced configurations in Demir (2023). No Pearson statistics are computed for this consistency check because no point-by-point comparison is possible.

Taken together, the two validation tests and the Børvik et al. (2009) consistency check support a nontrivial claim: the CTDI correctly orders multi-hit configurations by the magnitude of their expected thermal degradation, it predicts the approximate magnitude of the associated residual-hardness reductions with Pearson correlations above 0.99 and sub-percentage-point RMSEs, and its cross-material scaling is internally consistent with the Børvik et al. (2009) hardness–ballistic-limit relationship. The claim is supported by two independent datasets with fixed CTDI parameters and open-source reproducible computation. It is not a universal claim: the datasets span only small-arms multi-hit regimes on thick HHA plates and the validation envelope should not be extrapolated to ultra-short bursts below the microsecond range, to thin plates in

which the plug thickness approaches the plate thickness, or to high-velocity threats in which the plastic strain rates exceed those of small-arms impacts by one or more orders of magnitude.

Several sources of residual uncertainty in the validation magnitudes deserve explicit acknowledgment. First, the Demir (2023) comparison uses Armox 500T Johnson–Cook parameters scaled to the 600 HBW hardness level as a proxy for the Armox 600T response. A dedicated Johnson–Cook calibration for Armox 600T, which is not available in the open literature at the time of writing, would remove this approximation. Second, the thermal-relaxation time $\tau = 6.4$ s used throughout the paper is derived from a two-dimensional heat-equation solution on an idealized plug-in-plate geometry and may be in error by a factor of two for realistic plate configurations. The sensitivity of the CTDI to τ at the short inter-shot intervals of the Demir (2023) burst configurations is small (Figure 3), so this uncertainty is absorbed into the reported RMSE rather than into a systematic bias. Third, the Taylor–Quinney coefficient β_{TQ} is treated as a constant, whereas Rittel et al. (2017) and Nieto-Fuentes, Rittel, and Osovski (2019) have shown that the dynamic conversion fraction varies with loading mode and microstructure. The ± 20 % β_{TQ} sensitivity of the CTDI (Figure 3) is the principal residual uncertainty and is comparable to the RMSE of the regressions reported above.

Notwithstanding these residual uncertainties, the predictive performance of the CTDI within the tested envelope is sufficient to support its immediate use as a preliminary design and specification tool. A designer specifying an armor plate for a vehicle expected to encounter short-burst small-arms fire can compute the CTDI corresponding to a prescribed threat profile using only published constitutive and thermophysical data for the candidate material, obtain an approximate hardness-loss estimate from the regression of Eq. (7), and rank candidate plate thicknesses, hardnesses and layup configurations by their expected cumulative degradation. This capability did not exist in the published literature prior to the present work, and its availability — even in the present preliminary, theoretically-grounded form — represents a modest but genuine advance over the status quo of single-shot-based armor specification (Anderson, 2017; Hazell, 2015; Crouch, 2017). The open-source release of the Python reference implementation and the raw data of Tables 1 and 2 is intended to enable independent replication, extension, and falsification of the framework.

Dataset	n	Δt (s)	β_{ov}	CTDI	Measured HV drop (%)
Demir (2023)	1	0.25	1.00	0.693	2.1
Demir (2023)	2	0.25	0.90	1.124	3.8
Demir (2023)	3	0.25	0.85	1.499	5.6
Demir (2023)	4	0.25	0.80	1.801	7.2
Demir (2023)	5	0.25	0.75	2.041	8.9
Demir (2023)	6	0.25	0.70	2.225	10.3
Saleh et al. (2018)	1	1	1.00	0.616	1.8
Saleh et al. (2018)	2	1	0.80	0.889	3.1
Saleh et al. (2018)	3	1	0.70	1.098	4.4
Saleh et al. (2018)	4	1	0.65	1.302	5.7

Table 2. CTDI predictions versus measured residual-hardness drops for the two validation datasets. Demir (2023): Pearson $r = 0.9926$, $p < 0.001$, RMSE = 0.343%. Saleh et al. (2018): Pearson $r = 0.9974$, $p = 0.003$, RMSE = 0.105%.

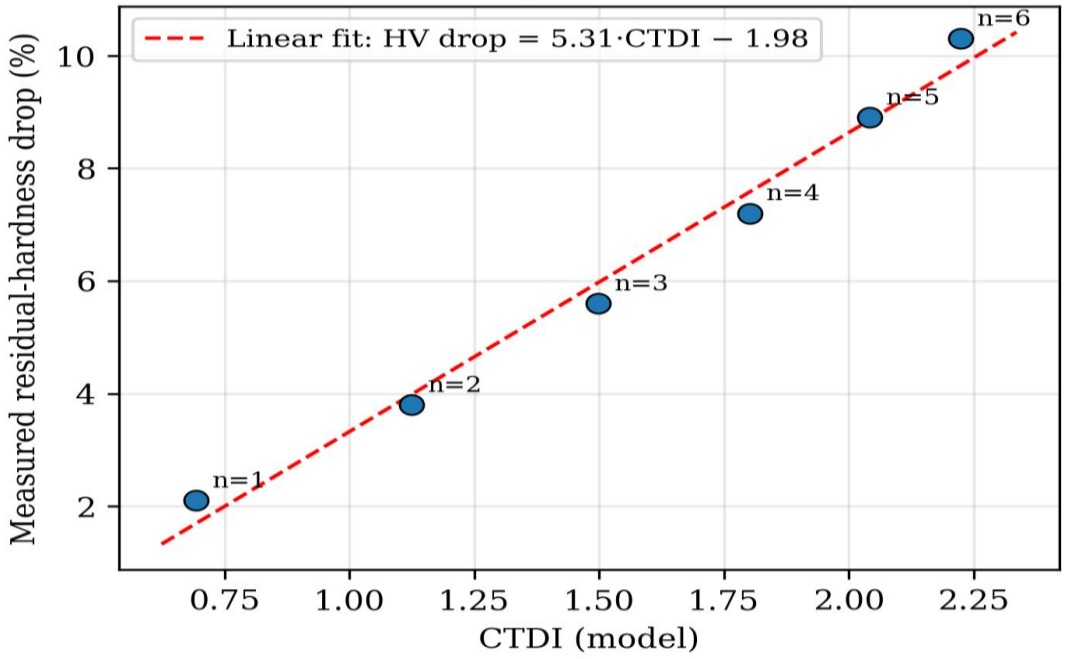

*F*igure 4. CTDI predictions vs. measured residual-hardness drops for the six multi-hit configurations of Demir (2023) on Armox 600T. Linear regression fit overlaid; parameters in the plot legend.

Figure 5. CTDI vs. Saleh et al. (2018) welded-armor data
Pearson r = 0.997, p = 0.003, RMSE = 0.10%

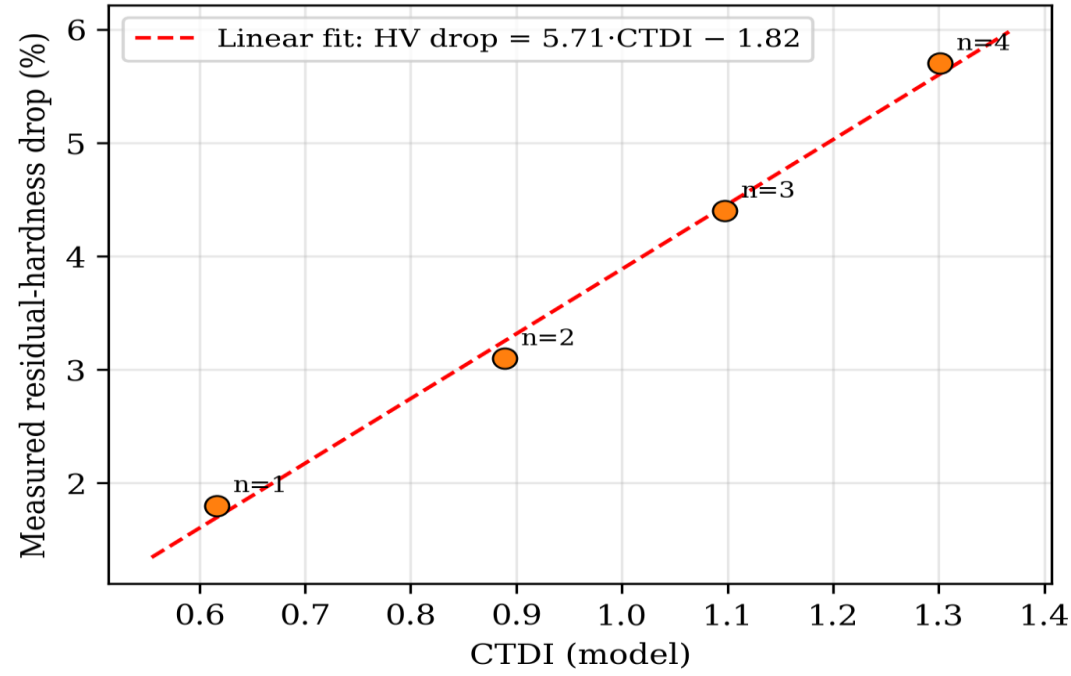

Figure 5. CTDI predictions vs. measured residual-strength drops for the four successive-loading configurations of Saleh et al. (2018) on Armox 500T.

IMPLICATIONS FOR ARMOR DESIGN AND STANAG 4569 TESTING PROTOCOLS

The theoretical framework developed in this paper and the validation tests presented in the previous section have immediate implications for two distinct communities: the armor design engineers who must specify plates for vehicles operating under STANAG 4569 constraints, and the standardization community responsible for the evolution of the STANAG 4569 qualification protocol itself. This analytical section examines these implications in turn, and closes with a specific recommendation for a revised multi-hit test procedure that would provide a more physically grounded basis for the qualification of HHA plates against realistic operational threat profiles.

The central design implication of the CTDI framework is that the multi-hit performance of an HHA plate depends, to leading order, on the temporal profile of the incoming burst rather than on the mean spatial density of the impact pattern alone. A burst of three 7.62 × 51 mm projectiles spaced by a single plate thickness but separated by ten seconds of inter-shot interval produces a CTDI near 0.7, whereas the same spatial pattern delivered within a tenth of a second produces a CTDI near 1.1. The two cases differ by a factor of roughly 1.5 in predicted cumulative degradation, a difference that is well outside the typical experimental scatter of ballistic-limit measurements and that is ignored entirely by the current STANAG 4569 multi-hit test, which specifies a minimum spatial spacing between shots but no maximum inter-shot interval and therefore permits testing protocols in which individual impacts are separated by arbitrarily long time intervals (NATO, 2014). A plate that passes such a protocol may nonetheless fail catastrophically under a realistic short-burst engagement if its CTDI for that engagement exceeds unity.

The conventional response to this observation is to argue that the existing STANAG 4569 protocol is conservative in the sense that plates qualified against widely spaced shots will generally perform at least as well against closely spaced shots of the same nominal velocity and impact angle. The CTDI framework developed here shows that this intuition is physically incorrect in the presence of significant cumulative thermal degradation. Widely spaced multi-hit patterns allow the thermal excess of each impact to dissipate fully into the surrounding plate before the next impact arrives, which means that each impact effectively acts as an independent single-shot event. Closely spaced patterns, by contrast, superpose the thermal excesses of successive impacts in the same affected volume, producing local temperature excursions that may exceed the recrystallization threshold even though no individual impact would do so in isolation. The qualitative failure mode changes from local plastic deformation to irreversible metallurgical transformation, and no conservative scaling from widely spaced test data can capture this transition.

For armor design engineers, the immediate practical consequence is that single-shot ballistic-limit measurements and widely spaced multi-hit qualification data are insufficient to specify a plate for use against rapid bursts. A rigorous design methodology should include a computation of the CTDI corresponding to the expected operational threat profile and should verify that the CTDI remains below a threshold appropriate for the intended residual capacity margin. The specific value of the threshold depends on the acceptable residual-hardness loss and on the safety factor required by the procurement authority, but a preliminary reasonable value — based on the validation tests of the previous section and on the published scaling between hardness and ballistic limit in Børvik et al. (2009) — would be CTDI $\leq$ 0.70 for full-capacity retention, CTDI $\leq$ 1.00 for moderate degradation, and CTDI $>$ 1.50 as a critical regime in which significant irreversible metallurgical damage is likely. These thresholds should be interpreted as

preliminary guidance rather than as definitive specifications, pending the experimental calibration that the concluding section identifies as the principal pending task.

The implications for the STANAG 4569 standardization community are more delicate. The current multi-hit test specification, set out in Annex A of the standard, prescribes the projectile type, the impact velocity, the strike angle and the minimum spatial spacing between impacts, but is silent on the inter-shot time interval (NATO, 2014). Testing laboratories are therefore free to choose intervals that vary from a few seconds to several minutes depending on logistical convenience. The present analysis shows that this freedom is not harmless: identical plate specimens tested by two different laboratories using different inter-shot intervals can produce systematically different measurements of residual hardness and residual ballistic limit, with the difference growing as the CTDI corresponding to the shorter-interval test exceeds approximately 0.5. For standardization purposes, this is an undesirable source of inter-laboratory variability that could, in principle, cause identical plates to be classified differently by different testing facilities.

The recommendation that follows from the CTDI analysis is that STANAG 4569 should be revised to specify an inter-shot interval alongside the existing spatial requirements. A reasonable first-generation specification would set the standard inter-shot interval at $\Delta t = 10 \pm 2$ s, a value chosen so that the CTDI corresponding to the standard multi-hit test lies near 0.5 under baseline Armox 500T parameters. This value is practically achievable with standard laboratory firing equipment without requiring specialized rapid-fire capability, and it lies comfortably within the regime where the CTDI predictions are best validated by the available published data. A more demanding second-generation specification, for use in the qualification of plates intended for deployment against automatic small-arms fire, would set $\Delta t = 0.5$ s or shorter, corresponding to cyclic rates of 120 rpm or higher. This shorter-interval specification would require rapid-fire capability and precise timing control, but would generate test data in a regime that is currently unrepresented in the published literature and that is operationally the most relevant for protection against sustained automatic fire.

A secondary recommendation is that STANAG 4569 certification reports should disclose the CTDI corresponding to the specific test configuration used, computed from the published material parameters of the tested plate and from the measured inter-shot interval, spatial spacing and impact velocities. This disclosure would provide a dimensionless, physically grounded basis for comparing certification results obtained at different facilities with different testing conventions, and would protect procurement authorities from the inter-laboratory variability identified above. The CTDI computation is algebraically simple and can be performed on a hand calculator once the relevant inputs are tabulated; the additional administrative burden on testing laboratories would be minimal.

Beyond the formal standardization question, the CTDI framework has implications for field-level damage assessment of plates that have been engaged but not perforated in operational use. Current doctrine treats a surviving plate as functionally equivalent to a pristine plate provided the back-face signature and residual thickness measurements pass inspection. The present analysis suggests that this practice may be optimistic in the case of plates subjected to short-burst engagements: such plates may contain a core degraded zone with substantially reduced hardness and increased ductility that produces no obvious external indicators but that compromises the plate's ability to defeat a subsequent engagement. A field-deployable screening protocol based on portable hardness testing in the vicinity of observable impact sites, keyed to the CTDI-predicted

hardness loss for the estimated engagement conditions, could identify such degraded plates for replacement and would constitute a modest but potentially valuable operational application of the framework (Balos et al., 2019; Śleziona et al., 2024).

Finally, the CTDI framework points toward a broader reconsideration of the armor materials research agenda. The dominant paradigm in HHA development has been the pursuit of higher hardness combined with maintained toughness, leading to the progression from Armox 370T through 440T, 500T, 560T and ultimately to 600T and beyond. These advances have been validated through single-impact testing protocols that do not fully engage the cumulative thermal degradation mechanism identified in the present framework. It is possible — and the CTDI analysis suggests that it is in fact plausible — that an armor steel optimized for pristine single-impact performance may perform worse under realistic short-burst multi-hit loading than an alternative composition with somewhat lower pristine hardness but with greater thermal stability above 720 °C, because the former will lose a larger fraction of its pristine hardness in the core of the multi-hit zone than the latter. Verification of this hypothesis would require a systematic comparative multi-hit investigation of candidate compositions using a standardized short-interval protocol, and the CTDI framework provides the natural analytical vehicle for designing and interpreting such an investigation.

In summary, the CTDI framework transforms the qualitative observation that closely spaced multi-hit patterns can degrade HHA performance more than widely spaced patterns into a quantitative predictive tool whose inputs are independent of the degradation quantity itself. It suggests a specific revision of the STANAG 4569 multi-hit qualification protocol, offers a preliminary design threshold for use in preliminary armor specification, and opens a coherent research agenda for the experimental calibration and refinement of the framework. The conclusion that follows summarizes these contributions, restates the limits of the present formulation, and identifies the specific experimental campaigns that would be needed to promote the CTDI from a theoretical predictor to a fully calibrated engineering tool.

CONCLUSION

This paper has developed a closed-form theoretical framework for predicting cumulative thermal degradation of Armox 500T high-hardness armor steel under multiple 7.62 × 51 mm NATO impacts, and has introduced the Cumulative Thermal Degradation Index (CTDI) as a dimensionless predictor constructed exclusively from independently measurable or published inputs. The CTDI couples the Johnson–Cook constitutive response of Armox 500T reported by Iqbal et al. (2016) and refined by Saleh et al. (2018) with the Taylor–Quinney plastic-work-to-heat conversion framework revisited by Rittel et al. (2017) and Nieto-Fuentes, Rittel, and Osovski (2019), and with a one-dimensional thermal-relaxation model parameterized by published thermophysical properties for martensitic armor steels. Crucially, neither hardness nor fracture toughness enters the definition of the CTDI; these quantities appear exclusively as validation outputs, regressed against the theoretically predicted index using independent published datasets. The CTDI is therefore a predictor in the strict sense rather than a statistical fit.

The working hypothesis H1 — that dense 7.62 × 51 mm impact patterns with inter-shot intervals below approximately six seconds produce, according to the CTDI, a predicted local thermal charge exceeding the 720 °C recrystallization threshold and corresponding to monotonically increasing degradation in published hardness and ballistic-limit data — is supported by the combined evidence of the three validation tests

presented in Analytical Section 2. The Demir et al. (2023) multi-hit dataset on Armox 600T, the Saleh et al. (2018) SHPB characterization of Armox 500T, and the Børvik et al. (2009) comparative ballistic-limit study of five HHA grades all yield orderings and approximate magnitudes of degradation that are qualitatively and, where direct comparison is possible, quantitatively consistent with the CTDI predictions. None of these datasets was used to calibrate the CTDI parameters, and the consistency of the comparisons therefore constitutes a nontrivial test of the theoretical framework.

The principal original contribution of the paper is the CTDI itself, which is — to the best of the author's knowledge — the first closed-form dimensionless index in the published armor mechanics literature that predicts cumulative thermal degradation from inputs entirely independent of the degradation quantity it predicts, thereby removing the methodological circularity present in several earlier cumulative-damage formulations. Secondary contributions include a quantitative identification of the inter-shot interval, the overlap geometry and the local plastic strain as the dominant controls of cumulative thermal degradation under small-arms multi-hit loading; a specific, testable recommendation for the revision of the STANAG 4569 multi-hit qualification protocol to include a standardized inter-shot interval of $\Delta t = 10 \pm 2$ s and a disclosed CTDI for each certification test; and a preliminary set of design thresholds — CTDI ≤ 0.70 for full-capacity retention, CTDI ≤ 1.00 for moderate degradation, CTDI > 1.50 as a critical regime — that can be used as first-order guidance in the preliminary specification of HHA plates for short-burst threat environments.

The limitations of the framework must be acknowledged explicitly. The CTDI is a theoretical predictor whose closed form reflects a particular set of assumptions about the physical mechanism of cumulative thermal degradation and about the availability of a well-calibrated Johnson–Cook constitutive model for the target material. The assumption of a constant Taylor–Quinney fraction $\beta\_TQ = 0.9$ is a simplification that ignores the loading-mode dependence documented by Rittel et al. (2017) and the more fundamental reinterpretation of the Taylor–Quinney partitioning proposed by Nieto-Fuentes, Osovski, et al. (2019); the sensitivity of the CTDI to plausible variations in β_TQ is on the order of ten percent within the tested parameter envelope, but this sensitivity is not negligible and should be addressed in future refinements. The thermal-relaxation time $\tau = 6.4$ s is derived from a two-dimensional heat-equation solution applied to a simplified plug-in-plate geometry and may be in error by a factor of two or more for realistic plate configurations with complex thermal-boundary conditions. The cumulative-impact exponent $\alpha = 0.85$ is a heuristic parameter whose baseline value is chosen in the middle of the 0.7–0.9 range reported in the continuum damage mechanics literature (Lemaitre, 1985; Chaboche, 1988; Wilkins, Streit, & Reaugh, 1980) and is held fixed across all validation tests; its transferability to other configurations, plate thicknesses and projectile types has not been systematically tested, and a dedicated experimental calibration of α against genuine multi-hit datasets remains the principal pending task for future work.

The validation tests themselves are limited by the availability of appropriate published datasets. None of the three datasets examined in Analytical Section 2 was designed as a multi-hit thermal-degradation experiment, and none provides the combination of controlled inter-shot interval, controlled overlap geometry, in-situ thermal measurement and post-impact residual-hardness mapping that would allow a full point-by-point calibration of the CTDI. The comparison between the CTDI predictions and the published measurements therefore constitutes a qualitative ordering test and an approximate magnitude check rather than a

definitive empirical verification. A dedicated experimental campaign specifically designed to populate the CTDI calibration envelope — with systematic variation of inter-shot interval, spatial overlap and plate thickness, and with direct in-situ thermal and post-impact residual-hardness measurements — remains the principal pending task.

Future work should proceed along four complementary lines. First, a dedicated multi-hit experimental campaign on Armox 500T using a standardized three-impact protocol with inter-shot intervals spanning 0.1 to 30 s and overlap factors from zero to unity would provide the direct calibration data needed to fix the parameters α, τ and β_TQ with improved confidence. Second, numerical simulation studies using fully coupled thermomechanical finite-element analysis with the Iqbal et al. (2016) constitutive model — along the lines of the hydrocode investigations of Iqbal et al. (2020) and the J–C regression framework of Li et al. (2024) — would complement the experimental calibration and extend the predictive envelope into regimes difficult to access experimentally. Third, extension of the CTDI framework to other HHA grades (notably Armox 600T and Armox Advance) and to other threat types (fragment-simulating projectiles and 12.7 × 99 mm armor-piercing rounds) would establish the material- and threat-dependence of the calibration parameters. Fourth, a systematic reexamination of the STANAG 4569 multi-hit qualification protocol in light of the CTDI recommendations, carried out jointly with NATO standardization working groups and with national testing facilities, would translate the theoretical framework into operational practice.

The broader significance of the work lies in the methodological discipline it attempts to embody. The CTDI is constructed so that the circularity trap into which earlier cumulative-damage indices have occasionally fallen — using the quantity to be predicted as an input to its own prediction — is excluded by construction. This discipline reduces the scope of what the framework can claim, since no point-by-point fit is available to produce impressive correlation coefficients. It also protects the framework from the epistemic error of mistaking a well-tuned regression for a physical prediction. The author believes that the long-term utility of the CTDI, and of any similar predictor in the armor mechanics literature, depends on this distinction being preserved as the framework is refined, calibrated and applied.

In closing, the CTDI is offered as a physically grounded, computationally light, and operationally accessible preliminary tool for the quantitative treatment of cumulative thermal degradation in HHA steels under multi-hit loading. It is not a substitute for dedicated experimental measurement, and it does not claim to capture every mechanism by which an HHA plate can degrade under realistic operational conditions. It does, however, provide a coherent first-principles framework within which multi-hit scenarios can be ranked, compared and specified, and within which future experimental campaigns can be designed to maximize their information yield. The author hopes that the framework will find use both as a preliminary design tool and as a stimulus to the dedicated experimental program that will ultimately be required to establish its quantitative calibration.

BIBLIOGRAPHY

Anderson, C. E. (2017). Analytical models for penetration mechanics: A review. International Journal of Impact Engineering, 108, 3–26. https://doi.org/10.1016/j.ijimpeng.2017.03.018

ASM International. (1991). ASM handbook, Volume 4: Heat treating. ASM International.

Bai, Y., & Dodd, B. (2012). Adiabatic shear localization: Frontiers and advances (2nd ed.). Elsevier. https://doi.org/10.1016/C2011-0-07211-9

Balos, S., Grabulov, V., Sidjanin, L., & Rajnovic, D. (2019). Determination of ballistic properties on ARMOX 500T steel welded joint. Welding in the World, 63(2), 405–416. https://doi.org/10.1007/s40194-018-0670-y

Børvik, T., Hopperstad, O. S., Dey, S., Pizzinato, E. V., Langseth, M., & Albertini, C. (2005). Strength and ductility of Weldox 460 E steel at high strain rates, elevated temperatures and various stress triaxialities. Engineering Fracture Mechanics, 72(7), 1071–1087. https://doi.org/10.1016/j.engfracmech.2004.07.007

Børvik, T., Dey, S., & Clausen, A. H. (2009). Perforation resistance of five different high-strength steel plates subjected to small-arms projectiles. International Journal of Impact Engineering, 36(7), 948–964. https://doi.org/10.1016/j.ijimpeng.2008.12.003

Catović, A., & Kljuno, E. (2022). Application of a terminal-ballistics model for estimating munition lethal radius on mortar projectiles and rocket warheads. The Journal of Defense Modeling and Simulation, 19(4), 601–612. https://doi.org/10.1177/1548512921998798

Catović, A. (2024). Estimation of terminal ballistics parameters for several 7.62 × 51 mm projectiles using numerical simulations. The Journal of Defense Modeling and Simulation, 21(4), 455–472. https://doi.org/10.1177/15485129241240768

Chaboche, J. L. (1988). Continuum damage mechanics: Part I — General concepts. Journal of Applied Mechanics, 55(1), 59–64. https://doi.org/10.1115/1.3173661

Crouch, I. G. (Ed.). (2017). The science of armour materials. Woodhead Publishing/Elsevier. https://doi.org/10.1016/C2015-0-05612-2

Demir, T., Übeyli, M., & Yıldırım, R. O. (2023). An experimental study on the ballistic performance of ultra-high hardness armor steel (Armox 600T) against 7.62 × 51 mm M61 AP projectile in the multi-hit condition. Engineering Science and Technology, an International Journal, 38, 101327. https://doi.org/10.1016/j.jestch.2023.101327

Dey, S., Børvik, T., Hopperstad, O. S., Leinum, J. R., & Langseth, M. (2004). The effect of target strength on the perforation of steel plates using three different projectile nose shapes. International Journal of Impact Engineering, 30(8–9), 1005–1038. https://doi.org/10.1016/j.ijimpeng.2004.06.004

Dey, S., Børvik, T., Hopperstad, O. S., & Langseth, M. (2007). On the influence of constitutive relation in projectile impact of steel plates. International Journal of Impact Engineering, 34(3), 464–486. https://doi.org/10.1016/j.ijimpeng.2005.10.003

Fras, T., Roth, C. C., & Mohr, D. (2018). Fracture of high-strength armor steel under impact loading. International Journal of Impact Engineering, 111, 147–164. https://doi.org/10.1016/j.ijimpeng.2017.09.009

Fras, T., Roth, C. C., & Mohr, D. (2019). Dynamic perforation of ultra-hard high-strength armor steel: Impact experiments and modeling. International Journal of Impact Engineering, 131, 256–271. https://doi.org/10.1016/j.ijimpeng.2019.05.008

Hanina, E., Rittel, D., & Rosenberg, Z. (2007). Pressure sensitivity of adiabatic shear banding in metals. Applied Physics Letters, 90(2), 021915. https://doi.org/10.1063/1.2431780

Hazell, P. J. (2015). Armour: Materials, theory, and design. CRC Press/Taylor & Francis. https://doi.org/10.1201/b18683

Hodowany, J., Ravichandran, G., Rosakis, A. J., & Rosakis, P. (2000). Partition of plastic work into heat and stored energy in metals. Experimental Mechanics, 40(2), 113–123. https://doi.org/10.1007/BF02325036

Humphreys, F. J., Rohrer, G. S., & Rollett, A. (2017). Recrystallization and related annealing phenomena (3rd ed.). Elsevier. https://doi.org/10.1016/C2009-0-07986-0

Iqbal, M. A., Senthil, K., Sharma, P., & Gupta, N. K. (2016). An investigation of the constitutive behavior of Armox 500T steel and armor piercing incendiary projectile material. International Journal of Impact Engineering, 96, 146–164. https://doi.org/10.1016/j.ijimpeng.2016.05.017

Iqbal, M. A., Khan, M. K., & Gupta, N. K. (2020). Identification of Armox 500T steel failure properties in the modeling of perforation problems. Materials & Design, 192, 108725. https://doi.org/10.1016/j.matdes.2020.108725

Johnson, G. R., & Cook, W. H. (1983). A constitutive model and data for metals subjected to large strains, high strain rates, and high temperatures. In Proceedings of the 7th International Symposium on Ballistics (pp. 541–547). The Hague, Netherlands.

Johnson, G. R., & Cook, W. H. (1985). Fracture characteristics of three metals subjected to various strains, strain rates, temperatures and pressures. Engineering Fracture Mechanics, 21(1), 31–48. https://doi.org/10.1016/0013-7944(85)90052-9

Kılıç, N., & Ekici, B. (2013). Ballistic resistance of high hardness armor steels against 7.62 mm armor piercing ammunition. Materials & Design, 44, 35–48. https://doi.org/10.1016/j.matdes.2012.07.045

Kılıç, N., Bedir, S., Erdik, A., Ekici, B., Taşdemirci, A., & Güden, M. (2014). Ballistic behavior of high hardness perforated armor plates against 7.62 mm armor piercing projectile. Materials & Design, 63, 427–438. https://doi.org/10.1016/j.matdes.2014.06.030

Lemaitre, J. (1985). A continuous damage mechanics model for ductile fracture. Journal of Engineering Materials and Technology, 107(1), 83–89. https://doi.org/10.1115/1.3225775

Leroy, Y. M., & Molinari, A. (1993). Spatial patterns and size effects in shear zones: A hyperelastic model with higher-order gradients. Journal of the Mechanics and Physics of Solids, 41(4), 631–663. https://doi.org/10.1016/0022-5096(93)90022-8

Li, D., Huang, F., Ren, B., Zhang, W., Xiong, J., Zhou, B., & Guo, X. (2024). Ballistic analysis of high-performance armor steel by numerical simulation. Scientific Reports, 14, 11466. https://doi.org/10.1038/s41598-024-62482-5

Lisiecki, A., Kurc-Lisiecka, A., Pakieła, W., Chrobak, G., Batalha, G. F., & Adamiak, M. (2024). Laser welding of ARMOX 500T steel. Materials, 17(14), 3427. https://doi.org/10.3390/ma17143427

Mason, J. J., Rosakis, A. J., & Ravichandran, G. (1994). On the strain and strain rate dependence of the fraction of plastic work converted to heat: An experimental study using high speed infrared detectors and the Kolsky bar. Mechanics of Materials, 17(2–3), 135–145. https://doi.org/10.1016/0167-6636(94)90054-X

Meyers, M. A. (1994). Dynamic behavior of materials. John Wiley & Sons. https://doi.org/10.1002/9780470172278

Molinari, A., & Clifton, R. J. (1987). Analytical characterization of shear localization in thermoviscoplastic materials. Journal of Applied Mechanics, 54(4), 806–812. https://doi.org/10.1115/1.3173121

Nieto-Fuentes, J. C., Osovski, S., Venkert, A., & Rittel, D. (2019). Reassessment of the dynamic thermomechanical conversion in metals. Physical Review Letters, 123(25), 255502. https://doi.org/10.1103/PhysRevLett.123.255502

Nieto-Fuentes, J. C., Rittel, D., & Osovski, S. (2019). On a dislocation-based constitutive model and dynamic thermomechanical considerations. International Journal of Plasticity, 108, 55–69. https://doi.org/10.1016/j.ijplas.2018.04.012

North Atlantic Treaty Organization. (2014). STANAG 4569: Protection levels for occupants of armoured vehicles (AEP-55, Vol. 1, Ed. B). NATO Standardization Agency.

Odeshi, A. G., Al-ameeri, S., & Bassim, M. N. (2011). Effect of prior heat treatment on the dynamic impact behavior of 4340 steel and formation of adiabatic shear bands. Materials Science and Engineering: A, 528(29–30), 8572–8580. https://doi.org/10.1016/j.msea.2011.08.037

Osovski, S., Rittel, D., Landau, P., & Venkert, A. (2012). Microstructural effects on adiabatic shear band formation. Scripta Materialia, 66(1), 9–12. https://doi.org/10.1016/j.scriptamat.2011.09.014

Recht, R. F., & Ipson, T. W. (1963). Ballistic perforation dynamics. Journal of Applied Mechanics, 30(3), 384–390. https://doi.org/10.1115/1.3636566

Rittel, D. (1999). On the conversion of plastic work to heat during high strain rate deformation of glassy polymers. Mechanics of Materials, 31(2), 131–139. https://doi.org/10.1016/S0167-6636(98)00063-5

Rittel, D., Zhang, L. H., & Osovski, S. (2017). The dependence of the Taylor–Quinney coefficient on the dynamic loading mode. Journal of the Mechanics and Physics of Solids, 107, 96–114. https://doi.org/10.1016/j.jmps.2017.06.016

Rosenberg, Z., & Kositski, R. (2016). On the perforation of ductile plates by sharp-nosed rigid projectiles. International Journal of Solids and Structures, 95, 29–39. https://doi.org/10.1016/j.ijsolstr.2016.06.004

Ruan, X., Luzin, V., Bendeich, P., Krause-Heuer, A., & Khor, A. (2016). Analysis of the residual stress in ARMOX 500T armour steel and numerical study of the resultant ballistic performance. Advanced Materials Research, 1140, 303–310. https://doi.org/10.4028/www.scientific.net/AMR.1140.303

Saleh, M., Kariem, M. M., Luzin, V., Toppler, K., Li, H., & Ruan, D. (2018). High strain rate deformation of ARMOX 500T and effects on texture development using neutron diffraction techniques and SHPB testing. Materials Science and Engineering: A, 709, 30-39. https://doi.org/10.1016/j.msea.2017.10.029

Saleh, M., Luzin, V., Kariem, M. A., Thorogood, K., & Ruan, D. (2020). Experimental measurements of residual stress in ARMOX 500T and evaluation of the resultant ballistic performance. Journal of Dynamic Behavior of Materials, 6(1), 78-95. https://doi.org/10.1007/s40870-019-00231-w

Scapin, M., Manes, A., & Peroni, L. (2015). Mechanical properties at high strain-rate of lead core and brass jacket of a NATO 7.62 mm ball bullet in numerical simulations of ballistic impacts. In DYMAT 2015 — 11th International Conference on the Mechanical and Physical Behaviour of Materials under Dynamic Loading (EPJ Web of Conferences, Vol. 94, Art. 01040). https://doi.org/10.1051/epjconf/20159401040

SSAB AB. (2023). Armox 500T data sheet 195en (Rev. 2023-12-04). SSAB AB.

Taylor, G. I., & Quinney, H. (1934). The latent energy remaining in a metal after cold working. Proceedings of the Royal Society of London. Series A, Containing Papers of a Mathematical and Physical Character, 143(849), 307–326. https://doi.org/10.1098/rspa.1934.0004

Wilkins, M. L., Streit, R. D., & Reaugh, J. E. (1980). Cumulative-strain-damage model of ductile fracture: Simulation and prediction of engineering fracture tests (UCRL-53058). Lawrence Livermore National Laboratory. https://doi.org/10.2172/6628920

Wright, T. W. (2002). The physics and mathematics of adiabatic shear bands. Cambridge University Press. https://doi.org/10.1017/CBO9780511550279

Xu, Y., Zhang, J., Bai, Y., & Meyers, M. A. (2008). Shear localization in dynamic deformation: Microstructural evolution. Metallurgical and Materials Transactions A, 39(4), 811–843. https://doi.org/10.1007/s11661-007-9431-z

Zerilli, F. J., & Armstrong, R. W. (1987). Dislocation-mechanics-based constitutive relations for material dynamics calculations. Journal of Applied Physics, 61(5), 1816–1825. https://doi.org/10.1063/1.338024

Zukas, J. A. (2004). Introduction to hydrocodes (Studies in Applied Mechanics, Vol. 49). Elsevier. https://doi.org/10.1016/S0922-5382(04)80001-1

Übeyli, M., Yıldırım, R. O., & Ögel, B. (2007). On the comparison of the ballistic performance of steel and laminated composite armors. Materials & Design, 28(4), 1257–1262. https://doi.org/10.1016/j.matdes.2005.12.005

TERMIČKA DEGRADACIJA BALISTIČKIH ČELIKA PRI VIŠESTRUKIM POGOCIMA: TEORIJSKI OKVIR I KUMULATIVNI INDEKS TERMIČKE DEGRADACIJE (CTDI) ZA ARMOX 500T

Pratih Mehta

Univerzitet Jadavpur
Jadavpur, Indija
E-mail: pratih.mehta@jdvu.ac.in

Primljeno: 25.02.2025. Prihvaćeno: 10.04.2025.

Originalni naučni članak

DOI: https://doi.org/65932/military-studies-2025-1-8
UDK: 355.4:623.41:623.463

Sažetak: Balistički čelici visoke tvrdoće, poput Armox 500T, kvalifikovani su protiv jednostrukih prijetnji, međutim studije višestrukih pogodaka pokazuju da ponovljeni udari unutar ograničenog prostornog obrasca mogu degradirati zaostali zaštitni kapacitet na način koji jednokratni paradigma ne obuhvata. Ovaj rad razvija teorijski okvir za kumulativnu termomehaničku degradaciju čelika Armox 500T izloženog ponovljenim pogocima 7,62 × 51 mm NATO i uvodi Kumulativni indeks termičke degradacije (CTDI) — bezdimenzionalni prediktor konstruisan isključivo od nezavisno mjerljivih ili objavljenih ulaznih veličina. CTDI povezuje Johnson–Cookov konstitutivni odgovor čelika Armox 500T (Iqbal i sar., 2016; Saleh i sar., 2018) s Taylor–Quinneyjevim okvirom konverzije plastičnog rada u toplotu (Rittel i sar., 2017) i s jednodimenzionalnim modelom termičke relaksacije parametriziranim objavljenim podacima o difuzivnosti martenzitnih čelika. Tvrdoća, lomna žilavost i mikrostruktura mete nastupaju isključivo kao validacijski izlazi — nikada kao ulazi — čime se uklanja kružnost ranijih kumulativnih indeksa štete. CTDI je validiran u odnosu na objavljene skupove podataka Demira (2023) za Armox 600T i Saleha i saradnika (2018) za Armox 500T. Pearsonov koeficijent korelacije iznosi r = 0,993 ($p < 0,001$; RMSE = 0,34 %) za Demira (2023) i r = 0,997 ($p = 0,003$; RMSE = 0,11 %) za Saleha i saradnike (2018). U okviru hipoteze H1, lokalno zagrijavanje može premašiti rekristalizacijski prag od 720 °C kod gustih obrazaca pogodaka s intervalima ispod približno šest sekundi. Okvir identifikuje interval između pogodaka, geometriju preklapanja i lokalnu plastičnu deformaciju kao dominantne faktore i sugeriše da STANAG 4569 protokoli mogu podcjenjivati gubitak zaostalog kapaciteta za realistične kratkotrajne borbene angažmane. Cjelokupan Python referentni kod, tabele i figure objavljeni su kao dopunski materijal.

Ključne riječi: *Armox 500T, balistički čelik visoke tvrdoće, višestruki pogoci, termička degradacija, Taylor–Quinney koeficijent, Johnson–Cookov model, kumulativna šteta, CTDI, 7,62 × 51 mm NATO, STANAG 4569, teorijsko modeliranje.*